RSC Advances

PAPER

View Article Online
View Journal | View Issue

Check for updates

Cite this: *RSC Adv.*, 2023, **13**, 5643

Synthesis of Fe-THC MOFs and functionalizing MOFs by MXenes for the selective removal of lead(II) ions from wastewater†

Irfan Ijaz, *[a] Aysha Bukhari,[a] Ezaz Gilani,[a] Ammara Nazir[a] and Hina Zain[b]

The elimination of heavy metals, especially lead, from wastewater is vital for the environment and human health and using a proper adsorbent to achieve this goal is highly desirable. Initially, Fe-THC MOF was prepared using a simple method and functionalized using MXene for efficient, rapid, and selective elimination of lead. Different characterization tools demonstrated that Fe-THC MOF and its composite Fe-THC/MXene were successfully prepared. The adsorption outcomes showed that the maximum sorption capability was 674 mg g^{-1} at 305 K and pH 4.5. The sorption kinetics obeys the pseudo-second-order kinetic model, and the sorption isotherms fit the Langmuir isotherm model. This finding suggests monolayer sorption on Fe-THC/MXene, and the rate-controlling step is chemisorption. Thermodynamic findings exhibit that sorption was a spontaneous and exothermic process. The sorption process can selectively adsorb Pb ions from aqueous media. After five adsorption–desorption tests, the adsorption efficiency of Fe-THC/MXene was still high. The sorption mechanism of lead on Fe-THC was mainly due to the interaction of lead ions with –F and –O ions and porosity of the Fe-THC/MXene composite. The –O and –F ions were derived from MXene, while the porosity was derived from the MOFs of composites. These findings confirmed that Fe-THC/MXene enables rapid, efficient, and selective elimination of lead from wastewater, which is of practical importance.

Received 19th December 2022
Accepted 30th January 2023

DOI: 10.1039/d2ra08102d

rsc.li/rsc-advances

Open Access Article. Published on 15 February 2023. Downloaded on 2/4/2026 7:15:08 PM.
This article is licensed under a Creative Commons Attribution-NonCommercial 3.0 Unported Licence.

1. Introduction

Water is a necessary and planned resource that ensures economic and social development. The quick growth of the economy, remarkable growth of population, steady growth of several industries, and human activities are sources of environmental pollution, especially water pollution. Different industries, involving electrification, tanneries, mining, metal processing, smelting, battery production, *etc.*, have generated huge amount of heavy metals in wastewater.[1–4] Heavy metal wastewater is present in the environment in the form of direct or indirect approaches, such as river sediment, rainfall-runoff, domestic, industrial, and agricultural effluents, and atmospheric deposition.[5–8] Bulgariu *et al.* presented that numerous heavy metals are carcinogenic and toxic.[9] Nezamzadeh *et al.* identified that heavy metal pollution has already been extremely risky to the environment.[10] Lead is the most ordinary heavy metal in waste aqueous media. Excessive uptake of lead can induce intense injury to the kidney, nervous system, reproductive system, brain, and liver.[11,12]

Thus, the elimination of Pb from contaminated water is an essential job. Different approaches, such as electrochemical separation, ion exchange, adsorption, membrane process, distillation, advanced oxidation, and solvent extraction, have been reported for the elimination of Pb^{2+} ions.[13–16] All the above-mentioned approaches have certain disadvantages, such as high cost, difficulty of operation, and energy intensity. Among the above approaches, the adsorption approach has received tremendous attention due to its high efficiency, simplicity, ease of operation, cost efficiency, and high flexibility.[17,18] The choice of sorbents is a vital parameter in the sorption approach. Several sorbents, such as biomaterials, zeolites, metal oxides, activated carbon, bio-sorbents, and activated alumina clay, have been extensively utilized for Pb^{2+} ion removal.[19–21] Furthermore, all of these traditional sorbents exhibited low adsorption capacity for Pb removal.[22]

Two-dimensional materials have been utilized to remove heavy metals, dyes, and pharmaceuticals from wastewater *via* the adsorption technique. MXene is a well-known 2D material.[23] MXene contains transition metal nitrides, carbides, and carbonitrides and is a novel 2D material family that has drawn considerable attention these days. $M_{n+1}X_n$ is the general formula for MXene, where $n = 1$, 2, 3, and M correspond to

[a]*School of Chemistry, Faculty of Basic Sciences and Mathematics, Minhaj University Lahore, Lahore 54700, Pakistan. E-mail: iffichemixt266@gmail.com*

[b]*Department of Allied Health Sciences, Superior University Lahore, Lahore 54700, Pakistan*

† Electronic supplementary information (ESI) available. See DOI: https://doi.org/10.1039/d2ra08102d

© 2023 The Author(s). Published by the Royal Society of Chemistry

Open Access Article. Published on 15 February 2023. Downloaded on 2/4/2026 7:15:08 PM. This article is licensed under a Creative Commons Attribution-NonCommercial 3.0 Unported Licence.

transition metals like Nb, V, Ti, Sc, Mo, Zr, Ta, and Hf while X is N or C.[24] MXenes are mostly prepared using selectively etching Al from the MAX phase, where the A layers represent Ga, Al, or Si. After etching, the surface of MXene becomes rich in –F, –O, and –OH. As an adsorbent having the ability for environmental remediation, its outer surface has –F, –O, and –OH groups, so it can have better dispersibility in aqueous media and easily attract or bind the cationic heavy metals in water *via* electrostatic sorption.[25–27] For instance, Ying *et al.* introduced 2D MXene nanosheets for the removal of chromium.[28] Dong *et al.* reported the preparation of MXene/Alginate composite and investigated their adsorption activity against lead and copper. The prepared composite indicated an enhancement in adsorption capacity due to the increase in the active adsorption site.[29] Zhang *et al.* reported the synthesis of MXene@Fe_3O_4 composite and utilized it for the removal of methylene blue.[30]

Metal–organic frameworks are porous and crystalline structures consisting of a 3D network of cationic metal held in a specific position using organic molecules by coordination interaction, producing a cage-like network.[31] Because of their hollow, highly organized structure, MOFs have an impressively high internal surface area that is more than that of activated carbons, ranging from 1000 to 10 000 $m^2\ g^{-1}$. Many MOFs show excellent chemical stability in the presence of an extreme environment.[32] Additionally, MOFs can be prepared at a low cost and simple approach on a large level. The tunable physiochemical traits, along with highly organized material, make MOFs a favorable sorbent that is efficient in heavy metal ion removal.[33] Xu *et al.* described the synthesis of Zn/Zr-based MOFs by reaction of carboxyl/thiol or carboxyl/thiol-ether, which exhibited favorable adsorption performance for heavy metals (He *et al.*, 2011). Similarly, an azine-decorated Zn(II) MOF was investigated as a sorbent to trap heavy metal ions (Tahmasebi *et al.*, 2015). However, these virgin MOFs exhibited low adsorption capacity. To increase the adsorption capacity of heavy metal ions from drinking water, several MOFs have been modified by different researchers and scientists (Nozohour Yazdi *et al.*, 2018) (Yu *et al.*, 2018).[34] Thus, initially, in the current study, THC MOFs were synthesized, and then, the prepared THC MOFs were functionalized using MXene to increase the adsorption capacity. Herein, the basic objective of this work is to rapidly remove lead from wastewater to make it potable using a novel adsorbent. In order to prepare such adsorbents, first, we prepared **Fe-THC MOFs** from tetrahydrocannabinol, and then we prepared MXene from Ti_3AlC_2 *via* a wet chemical approach. Then, two different types of materials were combined to create novel Fe-THC/MXene composites as an adsorbent. The prepared THC/MXene composites exhibited excellent adsorption capacity against lead. Furthermore, suitable sorption conditions such as initial lead dosage, sorbent concentration, adsorption time, temperature, and pH were investigated carefully. The sorption kinetic and isotherm models were utilized to investigate adsorption phenomena, and FTIR, EDX, XRD, and XPS spectra were utilized to explore the adsorption mechanism.

2. Materials and methods

2.1. Materials used for this research

MAX (98%) powder was bought from 11 Technology (China). All of the chemicals used in this research are of analytical grade. Sodium hydroxide (NaOH), ferric chloride ($FeCl_3$, 98%), hydrochloric acid (HCl), tetrahydrocannabinol (**THC**), and hydrofluoric acid (HF) were obtained from Sigma-Aldrich and utilized without any purification.

2.2. Synthesis of Fe-THC MOFs

Initially, 256.7 mg of iron chloride was weighed and added to 100 mL of deionized water to make an aqueous solution. Then, 2 mmol solutions of tetrahydrocannabinol (THC) were prepared and mixed in the ferric chloride aqueous solution with continuous stirring, and the resultant solution was termed 1. 2 mol L^{-1} solution of sodium hydroxide was prepared and gradually dissolved in solution 1. The resultant solution was left for 60 min at 70 °C to make TCH react with Fe completely. When the above-formed solution was slowly cooled down at room temperature, a greenish-black powder was achieved after filtration and was immersed in deionized water for 6 h to let the impurities completely dissolve in the water. To remove all impurities from **Fe-THC MOFs**, the filtration and immersion process was replicated another 3 times. In the end, the prepared Fe-THC MOF was rinsed with ethanol and dried at 100 °C.

2.3. Synthesis MXene

Multilayered Ti_3C_2 (MXene) was prepared using a wet-chemical approach,[35] in which HF solution was employed as the etchant. Ti_3AlC_2 fine powder was dissolved in hydrofluoric acid and continuously stirred for 56 hours at 65 °C. The precipitates obtained from the above reaction were centrifuged and thoroughly washed with water 3 times. Finally, the wet solid residue (MXene) was dried at 70 °C for 20 h.

2.4. Synthesis of Fe-THC/MXene composites

The dispersion of MXene was sonicated for 1 h, and the pre-prepared 3 g of Fe-THC MOF was added to the dispersion of MXene. The resultant mixture was again sonicated for 20 min to obtain Fe-THC/MXene. The prepared Fe-THC/MXene was cleaned with ethanol solution and dried at 60 °C. The possible mechanism of the formation of the Fe-THC/MXene composite is exhibited in Fig. 1.

2.5. Characterization

The diffraction spectra for the composite were determined by an X-ray diffractometer (XRD; DX-100). Fourier transform infrared (FTIR) patterns were obtained using Nicolet iSO 20. The Raman spectra of the composite were investigated by a Raman spectrometer. The Brunauer–Emmett–Teller (BET) pore structure and surface area were determined using ASAP2460 (Micromeritics) by N_2 adsorption and desorption approach. The morphologies of composites were manifested using a scanning electron microscope (SEM; Hitachi S-4800) and a transmission

© 2023 The Author(s). Published by the Royal Society of Chemistry

Open Access Article. Published on 15 February 2023. Downloaded on 2/4/2026 7:15:08 PM.
This article is licensed under a Creative Commons Attribution-NonCommercial 3.0 Unported Licence.

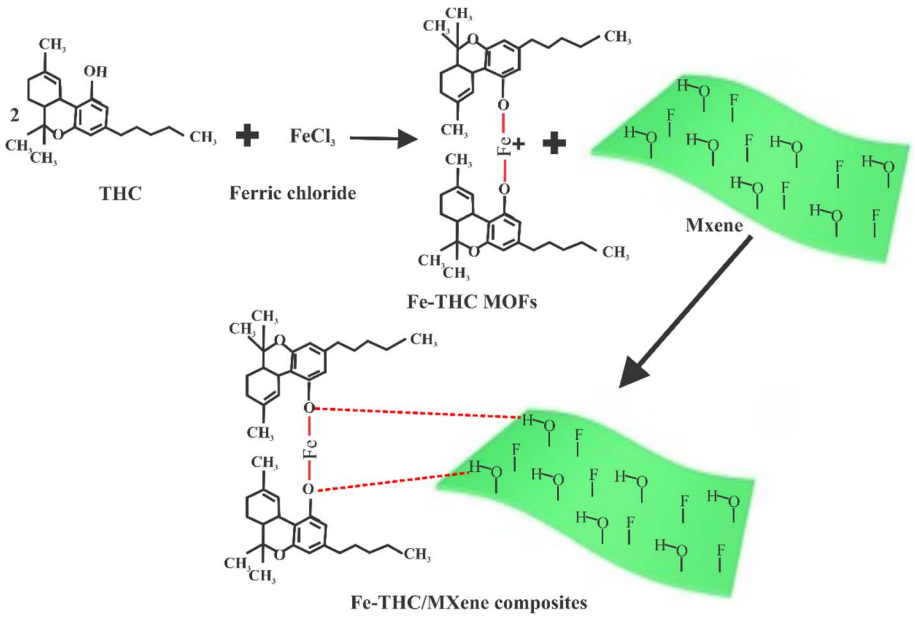

Fig. 1 Possible mechanism of formation of Fe-THC/composite.

electron microscope (TEM; JEOL JEM-2100HR). Energy dispersive X-ray (EDX) was utilized to determine the elemental composition. X-ray photoelectron spectroscopy (XPS, Thermo Scientific ESCALAB 250 Xi) was used to determine the chemical environment of materials.

2.6. Batch experiment

This investigation explored the adsorption activity of Fe-THC/MXene for Pb^{2+} ions under several initial concentrations, reaction time, temperature, and pH. In the entire investigation, the adsorption was conducted at 305 K. The temperature effect experiments were conducted at different temperatures (305, 310, and 315 K), and the ratio of sorbent (mg) to the solution (mL) was (1 : 1). The Pb^{2+} ion solution comprised lead nitrate and deionized water and the obtained data of all solutions were calculated using ICP-AES. When investigating the impact of pH, NaOH and HCl (0.1 mol L^{-1}) were utilized to maintain the pH of the reaction solution (15 mg L^{-1}) from 1–8, and the lead ion solution and sorbent were dropped into the centrifuge tube for sorption reaction to measure the suitable pH value. The sorption kinetics at various lead initial concentrations (10, 20, and 30 mg L^{-1}) were investigated by setting various reaction times and determining the adsorption equilibrium time. To investigate the maximum sorption capability of sorbent, an isotherm study was performed in the range of initial lead ion dosage of 10–1000 mg L^{-1}. After stirring for 3 h, the solid residual Pb^{2+} ion dosage of the residual lead ion concentration of the supernatant was determined, and the sorption capability was measured. This work also investigates the reusability and selectivity of Fe-THC/MXene to Pb^{2+}. 75 mg of Fe-THC/MXene and 75 mL of the simulated aqueous solution were reacted for 24 h. ICP-AES was employed to measure the dosages of metal ions in the simulated wastewater before or after sorption. 75 mg of Fe-THC/MXene and 75 mL Pb^{2+} solution were stirred for 24 h. After the isolation of liquid and solid, the desorption process was applied with 15% thiourea and 5% HCl for 24 h. The adsorbent (Fe-THC/MXene) was rinsed thrice with deionized water to neutrality after each desorption.

The adsorption capability and removal rate of Pb(II) were described by eqn (1) and (2),

$$q_e = \left(\frac{C_o - C_e}{M}\right) V \quad (1)$$

$$R = \left(\frac{C_o - C_e}{C_e}\right) \times 100 \quad (2)$$

where q_e defines adsorption capability (mg g^{-1}), C_o describes the initial concentration (mg L^{-1}) of lead(II) before adsorption, and C_e/C_t describes the remaining or final concentration (mg L^{-1}) of lead(II) ions after adsorption, R (%) describes the removal rate (%) of lead, m describes the mass of Fe-THC/MXene in mg, and V describes the volume of lead in L.

2.7. Adsorption kinetics

To investigate the adsorption kinetics of lead on Fe-THC/MXene composite, 20 mg Fe-THC/MXene composite and 20 mL lead solution with varying concentrations at pH 4.5 were allowed to react for a specific time (1–40 min, 10 to 30 mg L^{-1}). The derived information was fitted with intra-particle- diffusion (eqn (3), ID), pseudo-first-order (eqn (4), PFO), and pseudo-second-order (eqn (5), PSO).[36–38] The sorption mechanism of lead(II) on Fe-THC/MXene was derived *via* a comparative study.

$$q_e = K_3 t^{0.5} + C \quad (3)$$

$$q_e = (q_e - q_t) = \ln q_e - K_1 t \quad (4)$$

Open Access Article. Published on 15 February 2023. Downloaded on 2/4/2026 7:15:08 PM. This article is licensed under a Creative Commons Attribution-NonCommercial 3.0 Unported Licence.

$$q_e = \frac{t}{q_e} + \frac{1}{K_2 q_t^2} \quad (5)$$

where q_e (mg g^{-1}) describes adsorption capability at an equilibrium state and q_t describes the quantity of lead adsorbed at a specific time. K_{id} (mg g^{-1} $min^{-1/2}$), K_1 (min^{-1}), and K_2 (g mg^{-1} min^{-1}) are the rate constants of ID, PFO, and PSO, respectively, and C is a constant that describes the thickness of the boundary layer.

2.8. Adsorption isotherm

The isotherm investigation involves the reaction of 20 mg of Fe-THC and 20 mL of Pb solution for 24 h at a pH value of 4.5, and the lead dosage range was 10–30 mg L^{-1}, which were well-fitted using Langmuir, Freundlich, and Temkin isotherm models. The Langmuir isotherm model considers monolayer adsorption on the homogenous surface, defined as eqn (6).[39] The Freundlich isotherm model considers multi-layer sorption and is defined as eqn (7).[40] Temkin isotherm model considers that heat of sorption reduces with the interaction between the adsorbate (Pb^{2+}) and the adsorbent (FE-THC/MXene) and is defined as eqn (8).[41]

$$q_e = \frac{q_m K_L C_e}{1 + K_L C_e} \quad (6)$$

$$\Delta G = \Delta H + T\Delta S \quad (7)$$

$$q_e = \frac{RT}{B_T} \ln(K_T C_e) \quad (8)$$

Among all of these, q_m (mg g^{-1}) describes the maximum achieved sorption capability, K_L (L mg^{-1}) describes the Langmuir constant, and K_F ((mg g^{-1})/(mg L^{-1})$1/n$) defines the Freundlich equilibrium constant. K_T represents the Temkin constant, BT (J mol^{-1}) is connected to the heat of sorption phenomena, R describes the gas constant (J mol^{-1} K), and (K) describes temperature.

2.9. Thermodynamic study

To study the sorption of lead using Fe-THC/MXene at various temperatures, the thermodynamic factors were investigated at three different temperatures (305, 310, 315 K), including Gibbs energy (ΔG), entropy change (ΔS), and enthalpy (ΔH). If the adsorption capability decreases with an increase in temperature, the phenomenon is exothermic, and *vice versa*, an endothermic phenomenon occurs. The adsorption process is assumed to be spontaneous and feasible if a negative value of G is obtained. Eqn (9)–(11) were used for the calculations.

$$K_c = \frac{q_e}{C_e} \quad (9)$$

$$\ln K_c = -\frac{\Delta H}{RT} + \frac{\Delta S}{R} \quad (10)$$

$$\Delta G = \Delta H + T\Delta S \quad (11)$$

Among them, ΔH (kJ mol^{-1} K^{-1}), ΔG (kJ mol^{-1}), and ΔS (kJ mol^{-1}) indicate the enthalpy change, Gibb energy, and entropy change, respectively.

3. Result and discussion

3.1. Characterizations of Fe-THC MOFs, MXene, and Fe-THC/MXene composite

Fig. 2(a) shows the X-ray diffraction of the Ti_3AlC_2 (MAX) phase, **Fe-THC MOFs**, MXene, and Fe-TCH/MXene composite are exhibited. Initially, MXene sheets were produced by removing Al layers from the MAX (Ti_3AlC_2) phase with HF using chemical etching techniques described in prior research. This could be confirmed by the clear changes in the XRD spectrum (Fig. 2(a)). The (002) peak moved leftward with the vanishing characteristic peak of the MAX (Ti_3AlC_2) phase at 2θ around 39°, and a series of peaks (001) appeared. The characteristic bands of MXene at 2 theta (2θ) = 8.02°, 18.5°, 27.9°, 36.3°, and 60.7° bands were indexed to 002, 006, 008, 0010, and 100 planes, respectively, and agreed well with previous literature.[42,43] **Fe-THC MOFs** have the prominent band at 2 theta = 23° indexed to the 002 plane. XRD pattern of the Fe-TCH/MXene composite was well indexed with major peaks of MXene and **Fe-THC MOFs**. In other words, we can conclude that Fe-TCH/MXene composite displayed characteristic bands of MXene and **Fe-THC MOFs** with a higher intensity of some peaks. Furthermore, there was no specific peak of Fe in the Fe-TCH/MXene composite, suggesting a low dosage level of Fe in the composite.

FTIR protocol was performed to confirm the functional group of the substance. Fig. 2(b) indicates the FTIR spectrum of THC, **Fe-THC MOFs**, MXene, and Fe-TCH/MXEne. The FTIR pattern of **THC** had a prominent band at 3400 cm^{-1}, showing the stretching vibration of O–H,[44] which also ensured the presence of OH in **THC**. The band around 2909 cm^{-1} was indexed to the stretching vibration of CHs,[45] suggesting the presence of the CH group in **THC**. **THC** exhibited a band around 1051 cm^{-1},[46] indexing to the stretching vibration of CO. The band located at 1443 cm^{-1} indexed to an aromatic group, suggesting the existence of a benzene ring in THC.[47] In the FTIR pattern of Fe-THC, the OH peak vanished, which may be due to the removal of water as $FeCl_2$ interacts with THC. In the FTIR pattern of Fe-THC, one band was observed at 550 cm^{-1}, suggesting the presence of Fe–O bonds, which were not present in THC. In the FTIR pattern of MXene, the band at 2909, 1051, and 1443 cm^{-1} were present in both **THC** and **FE-THC MOFs**. The bands at 3428, 1389, 1092, and 658 cm^{-1} were indexed to the stretching vibrations of OH, C=O, OH, CF, and TiO functional groups that matched well with the reported results.[48] In the FTIR pattern of Fe-THC/MXene composite, the band at 3428(OH) came from MXene, which disappeared in the THC MOFs. Fe-THC/MXene had all major bands of THC MOFs and MXene.

The Raman pattern in Fig. 2(c) indicates two small peaks at 359 and 600 cm^{-1}, which were due to the vibrations of atoms in MXene and therefore indicated the successful preparation of MXene. Further, two wide bands were observed at about 1370 and 1579 cm^{-1}, designated as the D and G bands, respectively. A

© 2023 The Author(s). Published by the Royal Society of Chemistry

Open Access Article. Published on 15 February 2023. Downloaded on 2/4/2026 7:15:08 PM.
This article is licensed under a Creative Commons Attribution-NonCommercial 3.0 Unported Licence.

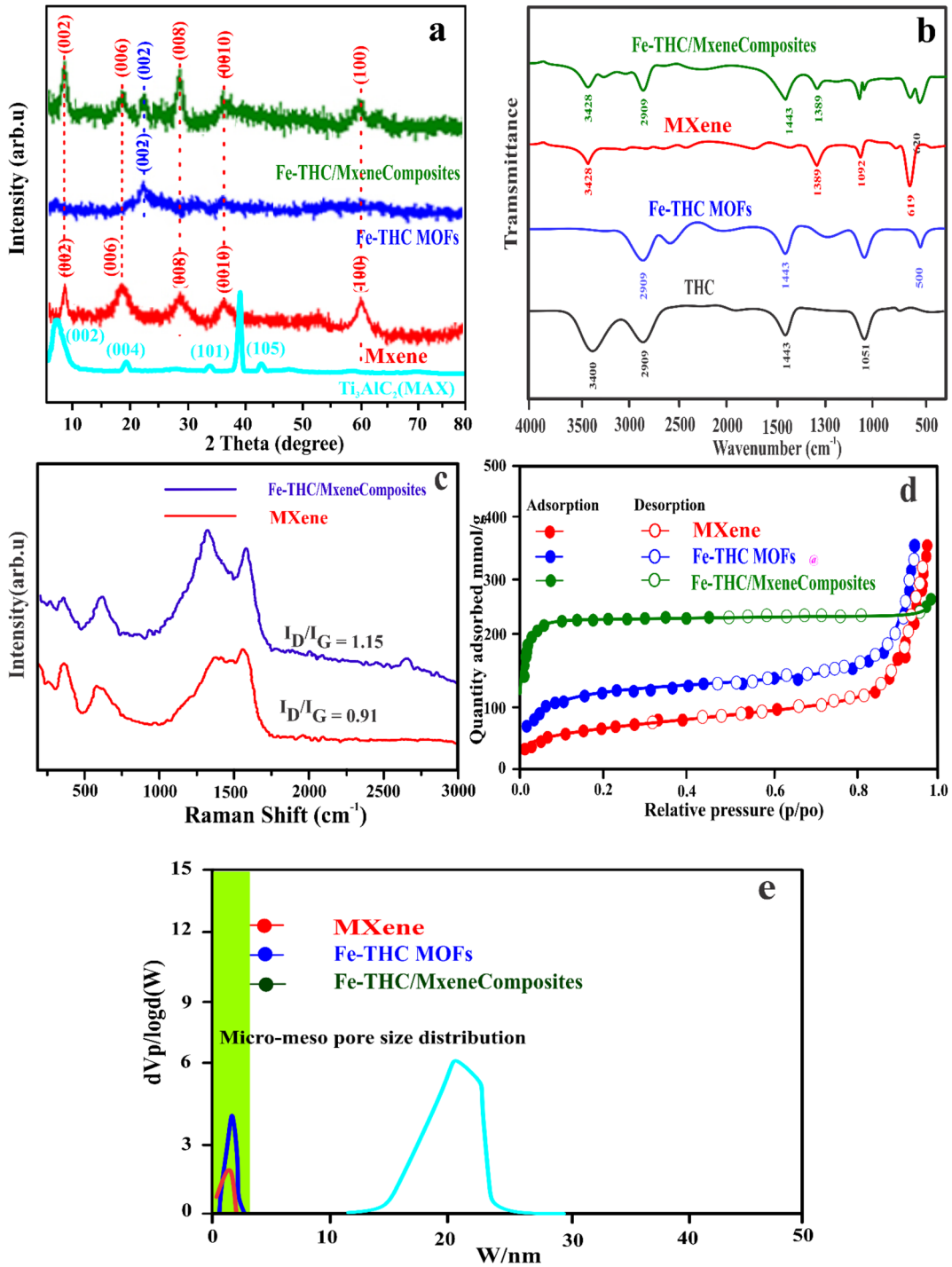

Fig. 2 FT-IR spectra (a), XRD analysis (b), Raman pattern (c), BET analysis (d), particle size distribution (e).

minor shift of the D band (nearly 50 cm^{-1}) was detected from the virgin MXene to the Fe-THC/MXene composite. This D-band shift was the defect's defining feature, which could be attributed to the $Ti_3C_2T_x$ interaction with the **Fe-THC MOFs**. It is also important to note that the I_D/I_G value showed a slight change after **Fe-THC MOFs** were added to MXene. This ratio increased from 0.91 to 1.15, suggesting more defects in the Fe-THC/MXene composite as compared to the original MXene.

Nitrogen adsorption–desorption isotherms of **Fe-THC MOFs**, MXene, and Fe-THC/MXene composites are displayed in Fig. 2(d). The BET isotherm of **Fe-THC MOFs** and MXene belonged to type II, and Fe-THC belonged to type IV classification, suggesting the microporous and mesoporous profile of **Fe-THC MOFs**, MXene, and Fe-THC/MXene composites. According to the nonlocal density functional theory (NLDFT) model, the pore size of MOFs was measured in the range of 0.2–1.8 nm,

Open Access Article. Published on 15 February 2023. Downloaded on 2/4/2026 7:15:08 PM.
This article is licensed under a Creative Commons Attribution-NonCommercial 3.0 Unported Licence.

while that of MXene was prominently about 0.1–1.7 nm. Compared to MOFs and MXene, the pore size of Fe-THC/MXene moved to the mesoporous range (12.0–29.4 nm), as shown in Fig. 2(e).

Electron microscopes (SEM and TEM) were employed to study the morphological features of as-prepared **Fe-THC MOFs**, MXene, and Fe-THC/MXene composites. The bare Fe-THC displayed a spherical and irregular-shaped structure (Fig. 3(a)). The bare MXene represented a layered structure (Fig. 3(b)). In comparison, SEM and TEM images of as-prepared Fe-THC/MXene (Fig. 3(c) and (d)) displayed clear anchoring of **Fe-THC MOFs** on the surface of MXene *via* electrostatic interaction. The presence of Ti, C, O, F, and in the EDX spectrum of the composite verified the synthesis of Fe-THC/MXene composites, as shown in Fig. 3(e).

3.2. Adsorption study

3.2.1. Influence of pH on lead adsorption. The pH value of the aqueous solution will affect the surface charge of the adsorbent and the adsorbate material.[49] Lead(II) is commonly available in the form of Pb^{2+} when pH is greater than 5.8, and $Pb(OH)_2$ and Pb^{2+} primarily exist between pH 5.8–7, and $Pb(OH)_2$ precipitates as pH crosses 7.[50] Thus, investigations were carried out in the pH range of 1–7. 20 mg of Fe-THC/MXene and 20 mL of Pb^{2+} ions solution were added to a centrifuge tube and reacted for 24 h. The finding is exhibited in Fig. 4(a) when pH varied from 4–7. The sorption capability is greater than 99%, and the sorption capability was lower before pH 4(a). The reason behind this finding is the competition of lead(II) ions for adsorption sites, which causes a reduction in its adsorption efficiency.[51] As the pH value increases from 4–7, the H^+ ion decreases and the competitive sorption of lead ions weakens, resulting in the increasing adsorption efficiency of Fe-THC/MXene. The influence of pH on the sorption phenomena of Pb^{2+} is associated with the surface charge of the adsorbent. It can be observed from Fig. 4(b) that the surface charge of Fe-THC/MXene slowly drops with the increase of pH until it becomes negatively charged. The point of zero potential for Fe-THC/MXene adsorbent is at pH = 6.58. The Fe-THC/MXene has a positive charge before 6.58 and becomes negative after 6.58. The point of zero potential is at pH = 6.55, and because of the

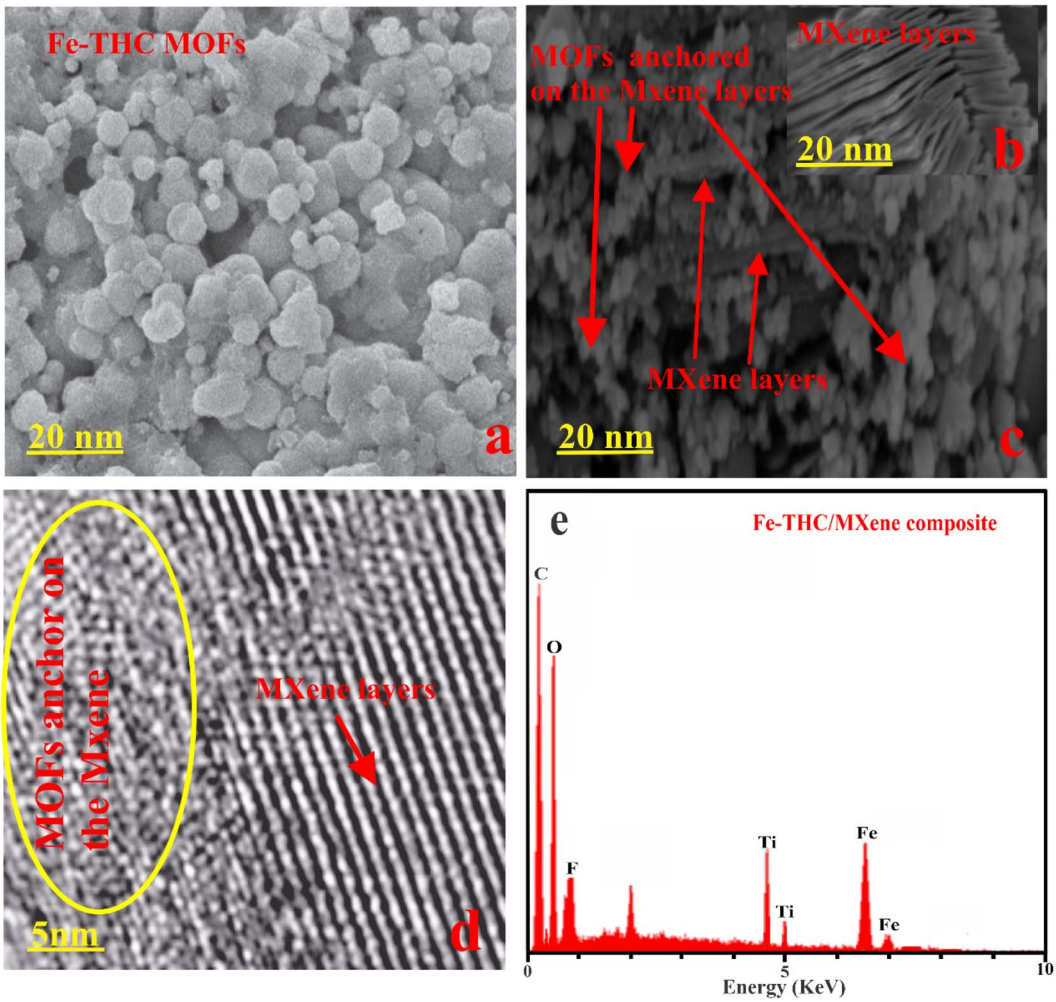

Fig. 3 SEM image of **Fe-THC MOFs** (a), MXene layered structure (b), and **Fe-THC MOFs** anchor on the MXene layered structure (c), TEM images of Fe-THC MOFs anchor on the MXene layered structure (d), and EDX spectrum (e) of composites.

© 2023 The Author(s). Published by the Royal Society of Chemistry

Open Access Article. Published on 15 February 2023. Downloaded on 2/4/2026 7:15:08 PM.
This article is licensed under a Creative Commons Attribution-NonCommercial 3.0 Unported Licence.

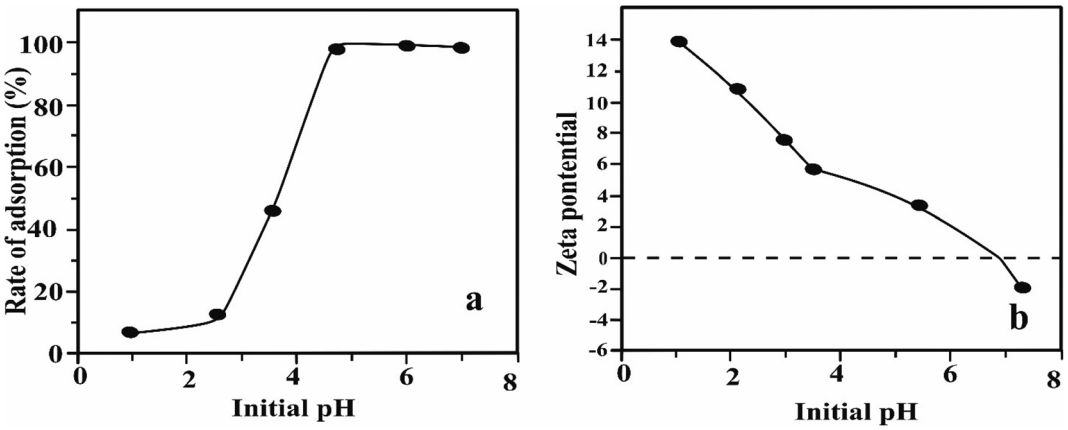

Fig. 4 Influence of pH on adsorption rate (%) (a) and zeta potential of Fe-THC/MXene composite (b).

pH value, insoluble $Pb(OH)_2$, will be formed.[52] To avoid this process, the sorption study was carried out under an environment of pH = 4.5. Below this pH, the surface of Fe-THC/MXene has a positive charge, which shows that there is no electrostatic disturbance in the sorption experiment.

3.2.2. Effect of adsorption time and kinetic analysis. Adsorption time is one of the essential factors for investigating the characteristics of adsorbents. Thus, this work reported the sorption equilibrium time at three different dosages (10, 20, and 30 mg L^{-1}) and analyzed its kinetics. The adsorption capability of lead(II) on the Fe-THC/MXene is exhibited in Fig. 5. The sorption capability of Fe-THC/MXene for lead(II) increased rapidly within 6 min, and the sorption capability enhanced slowly after 6–12 min (Fig. 5(a)). The sorption equilibrium was

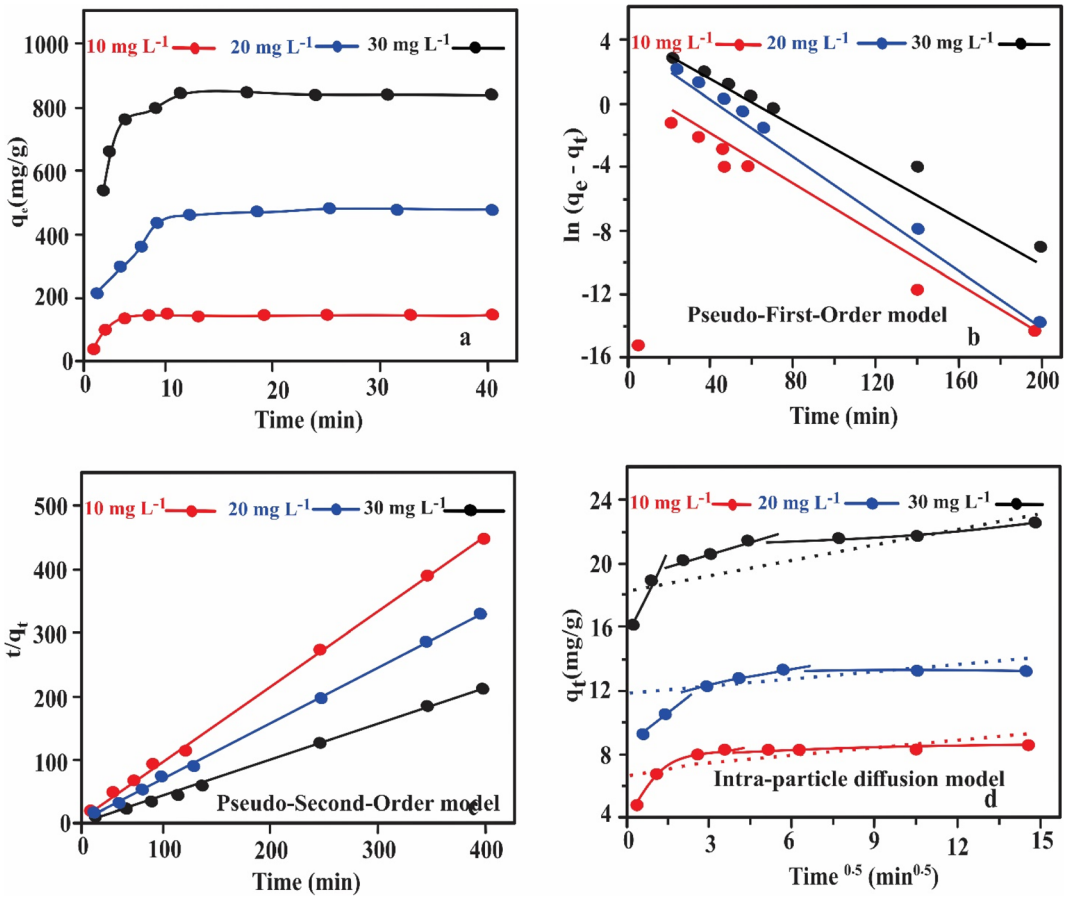

Fig. 5 Influence of Pb^{2+}adsorption time on Fe-THC/MXene (a), pseudo-first-order (b), pseudo-second-order (c), and intra-particle diffusion (d) models.

Open Access Article. Published on 15 February 2023. Downloaded on 2/4/2026 7:15:08 PM.
This article is licensed under a Creative Commons Attribution-NonCommercial 3.0 Unported Licence.

attained at 12 min. Such behavior in the initial stage was due to more sorption sites on the surface of the adsorbent, and the solution was composed of more lead(II), so the sorption rate was rapid. However, in the mid and later stages, the lead concentration in the solution slowly reduces, and the adsorption sites on the surface of the sorbent also slowly reduce, so adsorption attains an equilibrium state.

Through kinetic fitting of obtained experimental data, the sorption process of lead(II) on Fe-THC/MXene was attained. The kinetic parameters of three different kinetic models were derived by using the fitting results in Fig. 5(b–d) and Table S1.† It can be observed that the fitting results of the pseudo-second-order kinetic models have an extraordinarily high R^2 value at distinct initial lead(II) concentrations, greater than 0.9999, which is quite higher than the R^2 value of the pseudo-first-order kinetic model (0.9836). The related results and the fitting result of the pseudo-second-order sorption of lead on Fe-THC/MXene demonstrate the process of chemisorption.

In order to examine the intra-particle diffusion between adsorbate and lead sorption, the intra-particle diffusion kinetic model was also used. Fig. 5(c) exhibits the relationship between $t^{1/2}$ and q_t of lead concentrations on Fe-THC/MXene, which is non-linear over the whole adsorption time range. This suggests that the sorption phenomenon was not influenced by a single diffusion element.[53] There were three linear areas in the whole diffusion phenomena, which suggest surface sorption, intra-particle, and membrane diffusion termed I, II, and III, respectively. By studying the parameters of intra-particle diffusion by using three different concentrations in Table S2,† we can comprehend that the slope constant of the three areas is written as $K_I > K_{II} > K_{III}$, and intercepts are written as $C_I < C_{II} < C_{III}$.

3.2.3. Influence of initial concentration and adsorption isotherm. To explore the maximum sorption capability of Fe-THC/MXene composite for lead(II) was also examined. Fig. 6(a) displays the sorption capability of Fe-THC/MXene for lead(II) ions at three different temperatures 305, 310, and 315 K. As the initial dosage of lead(II) enhances, the sorption capability gradually rises until it attains saturation. The reason behind this behavior is that in a high lead concentration, the lead(II) ion will be accelerated to be adsorbed on the sorbent surface unless the sorption sites are entirely occupied to attain the sorption equilibrium state. The adsorption capacity of Fe-THC/MXene was higher at 305 K. It can be observed from the figure that as the temperature enhances, the sorption capability of Fe-THC/MXene composites for lead drops, which suggests the sorption phenomena is exothermic.

To investigate the role between lead and Fe-THC/MXene, this work selects three important isotherm models to fit the

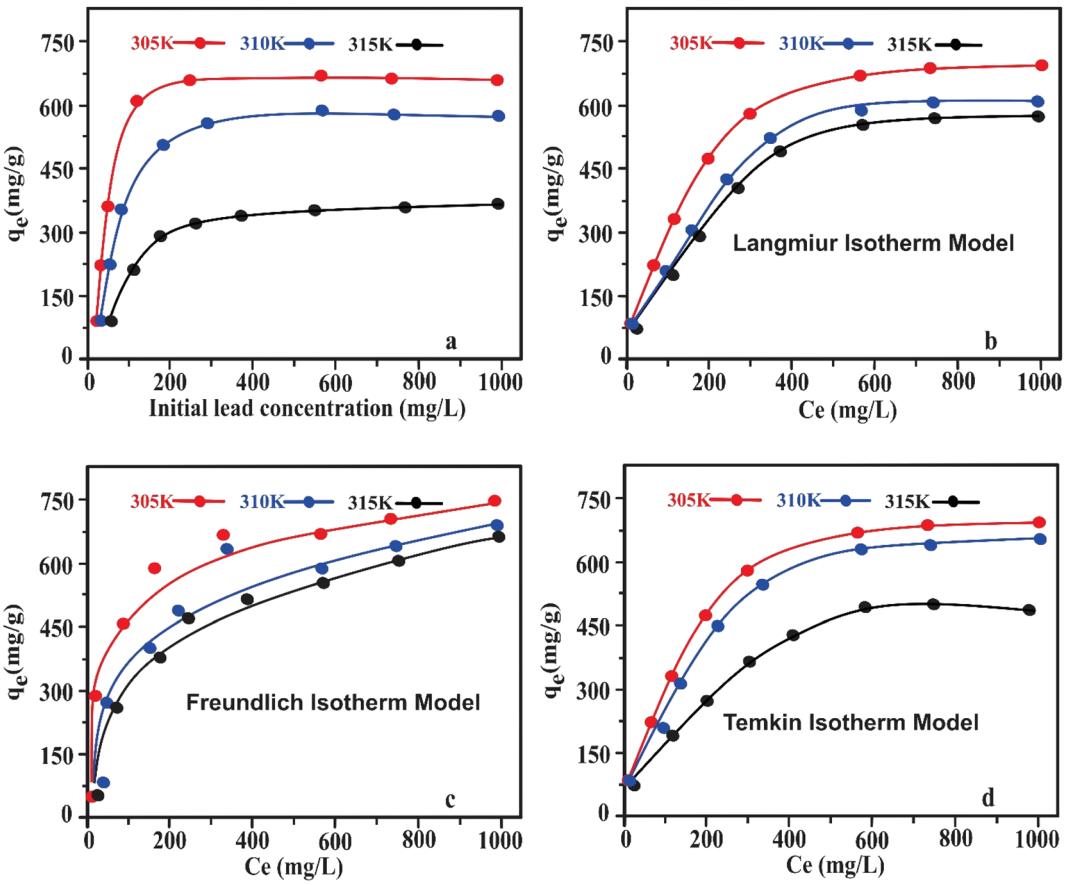

Fig. 6 Influence of Pb^{2+} concentrations on adsorption capability of Fe-THC/MXene (a), Langmuir (b), Freundlich (c), and Temkin (d) isotherm models.

© 2023 The Author(s). Published by the Royal Society of Chemistry

Open Access Article. Published on 15 February 2023. Downloaded on 2/4/2026 7:15:08 PM. This article is licensed under a Creative Commons Attribution-NonCommercial 3.0 Unported Licence.

obtained data. The fit information is exhibited in Fig. 6(b–d). The validity of the isotherm model is examined by comparing the R^2 value of each model. The higher the R^2 value, the more favorable the model is. By comparing the obtained results in the table, it can be concluded that under a distinct temperature environment, the Langmuir isotherm model has a higher R^2 value than the Temkin and Freundlich isotherm models. Table S3† suggests that the theoretical sorption capability derived by using the Langmuir isotherm model (q_e = 680, 298, and 84 mg g^{-1}) is closer to the sorption capability derived from experimental data (674, 293, and 77 mg g^{-1}). This suggests that the Langmuir isotherm model can better explain the sorption process of lead(II) on Fe-THC/MXene composites. The sorption of lead(II) on Fe-THC/MXene composite is monolayer sorption.[54] The Langmuir dimensionless parameter R_L, calculated from eqn (12), is used to investigate the feasibility of adsorption phenomena.

$$R_L = \frac{1}{1 + K_L C_o} \tag{12}$$

where C_o and K_L are the initial concentration of lead(II) and Langmuir isotherm constant, respectively. If $0 < R_L < 1$, it suggests that the sorption phenomenon of lead(II) on Fe-THC/MXene was conducted under a favorable environment. If $R_L > 1$, it suggests that the sorption phenomenon was conducted under unfavorable environments. By calculations, we determined that the R_L range of Fe-THC/MXene was 0.039 to 0.53, 0.039 to 0.63, and 0.067 to 0.73 at three distinct temperatures of 305, 310, and 315 K, respectively. R_L was between 0 and 1 for the three temperature environments. It exhibits that the sorption of lead(II) by Fe-THC/MXene was conducted under favorable environments.

3.2.4. Impact of temperature and thermodynamics analysis. The thermodynamic analysis results and related indicators are exhibited in Fig. 7(a) and (b) and Table S4.† ΔG is negative at three distinctive temperatures, and we can determine from Table S4† that the negative Gibbs free energy rises with a temperature rise, suggesting that the sorption phenomenon of lead on Fe-THC/MXene was spontaneous, and the temperature rise will decrease the sorption capability. The enthalpy value was greater than zero, suggesting that the sorption process is exothermic. A negative entropy value suggests that the disorder of the solid/liquid interface is lowered, and the sorption is conducted under adverse environments.

3.2.5. Selectivity and reusability of Fe-THC/MXene. The selective sorption of lead by Fe-THC/MXene in practical applications was analyzed utilizing simulated wastewater, and a comparative study was conducted with the selectivity of **Fe-THC MOFs** and MXene. The simulated wastewater consisting of Li(I), Ni(I), Cd(II), Cu(II), Mg(II), Pb(II), and Zn(II) was adjusted at pH = 5. 50 mg of sorbent and 50 mL of simulated wastewater solution were added into a centrifuge tube and reacted at 37 °C for 36 h, and the solid residue was isolated from the liquid. ICP-AES was utilized to measure the metal ion dosages before and after desorption. Fig. S1(a–d) and Table S5† indicate the sorption results of Fe-THC/MXene, Fe-THC, and MXene for each heavy metal in simulated wastewater. By comparison study, it can be observed that Fe-THC and MXene have a poor adsorption impact and selectivity on Pb(II) in simulated wastewater. Fe-THC/MXene composites are also selective on Pb(II), and the adsorption impact becomes higher than **Fe-THC MOFs** and MXene. The selectivity coefficient (K) and distribution coefficient (K_Q) were utilized to measure the selective sorption of lead in solution *via* the adsorbent. The greater the K_Q values, the stronger the relationship with the sorbent and the more useful the sorption impact. K exhibits the affinity of essential functional groups in Fe-THC/MXene composite, **Fe-THC MOFs**, and MXene to the mixed metal ion. The greater the value of K, the less the value of affinity. K and K_Q can be defined as

$$K = \frac{K_Q(Pb^{2+})}{K_Q(\text{coexitingions})} \tag{13}$$

$$K_Q = \frac{q}{C_e} = \frac{C_o - C_e}{C_e} \cdot \frac{V}{M} \tag{14}$$

The results are exhibited in Table S5.† For Fe-THC/MXene, Fe-THC, and MXene, the K_Q value of the lead ion is higher

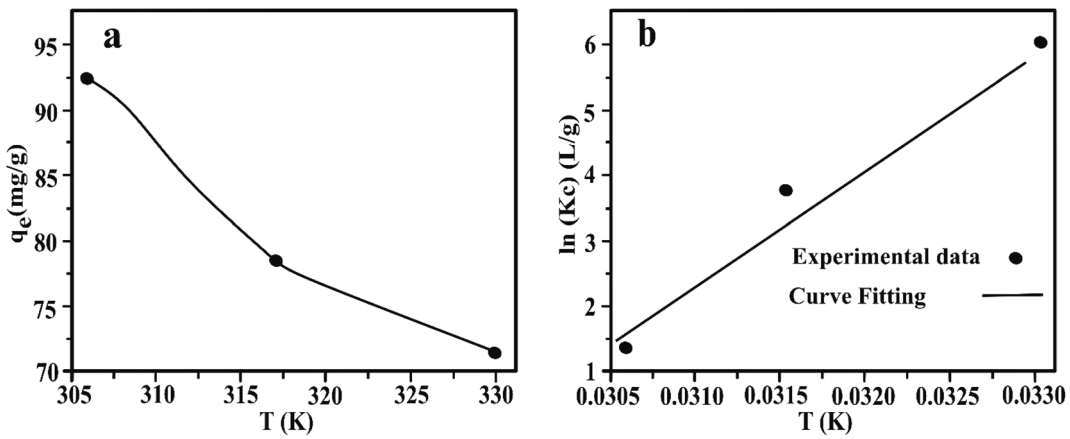

Fig. 7 Influence of temperature on adsorption capability of Fe-THC/MXene (a), and plot of ln K_c *versus* 1/T Langmuir (b).

Open Access Article. Published on 15 February 2023. Downloaded on 2/4/2026 7:15:08 PM.
This article is licensed under a Creative Commons Attribution-NonCommercial 3.0 Unported Licence.

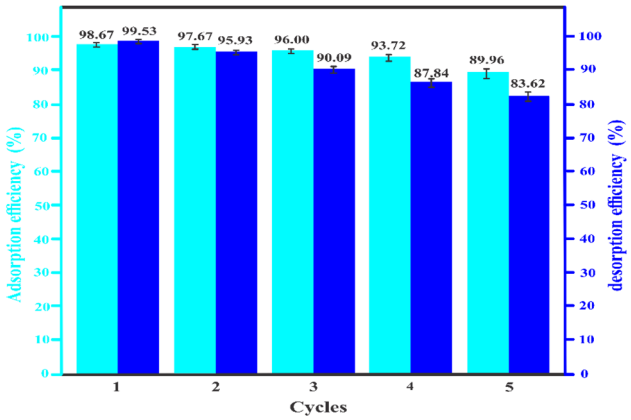

Fig. 8 Elimination efficiency of lead(II) after five adsorption–desorption cycles of Fe-THC/MXene.

than all other ions in the aqueous media, suggesting that interaction between the sorbents and lead ion is the strongest. Therefore, the removal rate of lead is higher than other heavy metal ions. The K_Q value of Fe-THC/MXene is more as compared to the K_Q value of **Fe-THC MOFs** and MXene, suggesting that Fe-THC/MXene exhibited a better sorption impact on lead. Fe-THC/MXene exhibited a higher K value for mixed ions, suggesting that the functional group showed less affinity for interfering ions. Comparatively, **Fe-THC MOFs** exhibited a greater value of K for mixed ions and showed more affinity for interfering ions. Collectively, Pb^{2+} ions in aqueous media can be efficiently and selectively eliminated by Fe-THC/MXene.

For practical uses, the expense of utilization should also be taken into account, and therefore, it is essential to investigate the reusability of Fe-THC/MXene. The testing results are displayed in Fig. 8. The sorption efficiency of the first repeated

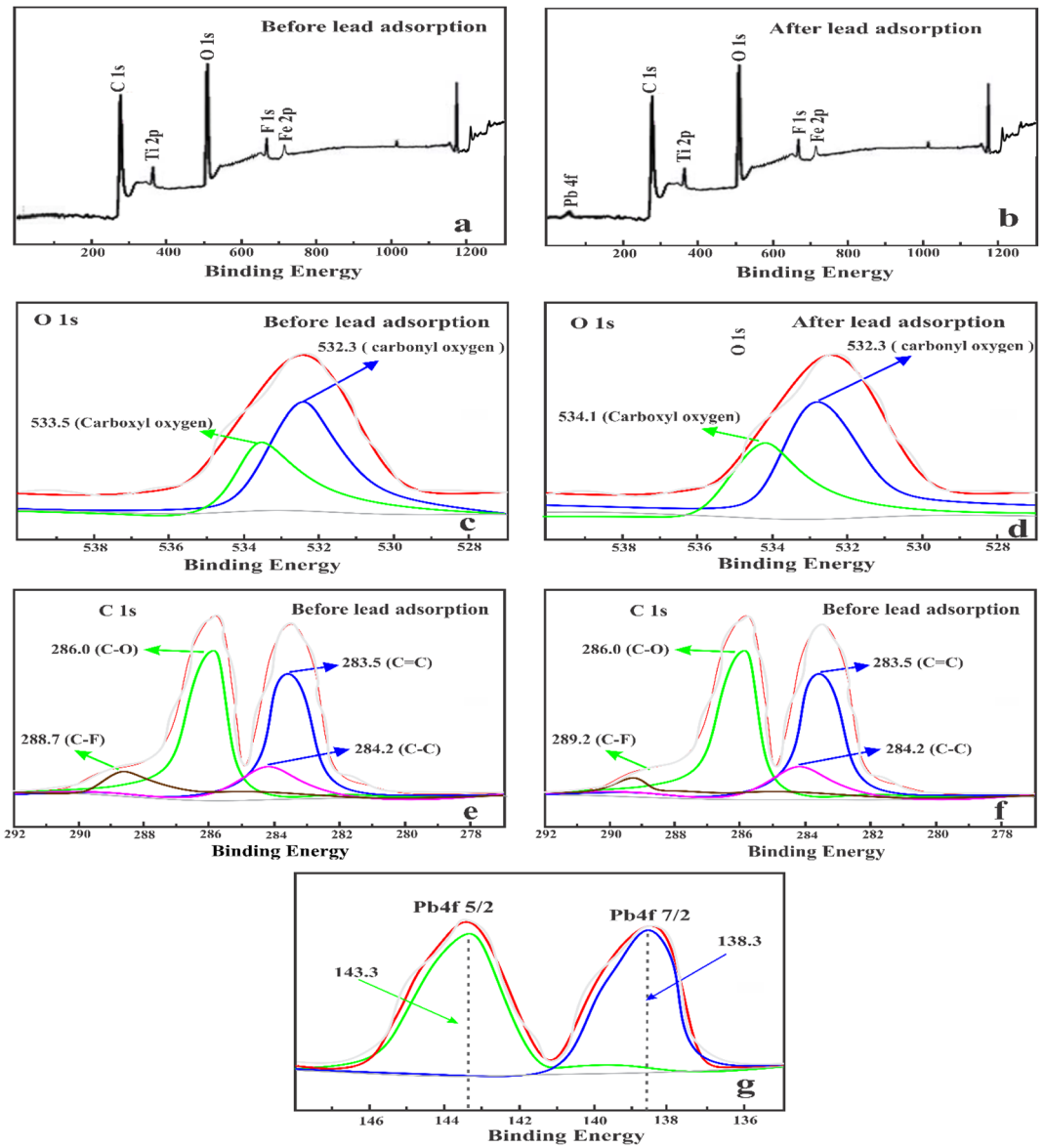

Fig. 9 XPS survey of Fe-THC/MXene before and after lead adsorption (a) and (b), O 1s (c) and (d), C 1s (e and f), and Pb 4f (g).

© 2023 The Author(s). Published by the Royal Society of Chemistry

Open Access Article. Published on 15 February 2023. Downloaded on 2/4/2026 7:15:08 PM. This article is licensed under a Creative Commons Attribution-NonCommercial 3.0 Unported Licence.

cycle achieved 98.67% and still retained 89.96% after five repeated cycles. Furthermore, the reusability tests also exhibit that Fe-THC/MXene can efficiently adsorb lead, and the desorption efficiency decreased only from 99. 53 to 83.62% after five consecutive cycles. This decrease in adsorption efficiency might be due to a decrease in –F and –OH ion dosage in adsorbents as the number of replications increases.

3.2.6. Adsorption mechanism. The sorption mechanism of lead on Fe-THC was investigated by estimating the XRD, EDS, FTIR, and XPS of Fe-THC/MXene after lead sorption. XRD pattern of Fe-THC/MXene after adsorption of lead is displayed in Fig. S2(a).† We can observe the XRD peaks of PbF_2 and PbO_2 along with that of Fe-THC/MXene. These results suggest that –F and –O on the adsorbent reacted with lead to form PbF_2 and PbO_2 in aqueous media for sorption. XRD pattern also exhibited that the diffraction peaks of Fe-THC/MXene after lead(II) adsorption were consistent with that before adsorption, suggesting that the crystal structure of sorbent (Fe-THC/MXene) was not disrupted after the lead sorption process. FTIR pattern of Fe-THC/MXene after adsorption of lead is exhibited in Fig. S2(b).† The FTIR pattern for lead(II) ion adsorbed Fe-THC/MXene displays the intensity of bands that were moved substantially lower as compared to Fe-THC/MXene, indicating the involvement of these functional groups in the attachment of lead(II) ions by Fe-THC/MXene. The intensity of Fe-THC/MXene moved from 3428 to 3451 cm^{-1} and from 1092 to 1102 cm^{-1} after lead ion sorption; these drops were attributed to fluoride (–F) and hydroxyl groups (–OH) involved in lead ion sorption on Fe-THC/MXene. EDX spectrum displayed the presence of Pb(II) ions along with Ti, C, O, F, and Fe, ensuring the adsorption of lead ions on Fe-THC/MXene (Fig. S2(c)†). XPS was utilized to determine the chemical elements and their binding energy on Fe-THC/MXene before and after sorption.

Fe-THC/MXene mainly consists of Ti, O, C, H, F, Fe, and Pb, and the presence of lead(II) also ensures the successful adsorption of lead ions on Fe-THC/MXene (Fig. 9(a) and (b)). After the adsorption of lead(II), the typical band of Pb 4f appeared. The Pb 4f band can be split into Pb 4f 5/2 (143.3 eV) and Pb 4f 7/2 (138.3 eV)[55,56] (Fig. 9(g)). The XPS pattern of O 1s before and after lead adsorption is exhibited in Fig. 9(c) and (d). The two basic bands around 532.3 and 533.5 eV appeared, relating to the carbonyl oxygen and carboxyl oxygen of the adsorbent, respectively.[57] The band relating to carboxyl oxygen (533.5 eV) was moved to 534.1 eV, while the band of carbonyl oxygen (532.3 eV) did not change its position. It means carboxyl oxygen on the surface of Fe-THC/MXene provided the binding sites for lead sorption. The four basic bands around 283.5, 284.2, 286.0, and 288.7 appeared, relating to the C=C, C–C, C–O, and C–F groups of the adsorbent, respectively (Fig. 9(e)). The band relating to C–F (288.7 eV) was moved to 289.2 eV, while the bands of C=C, C–C, and C–O did not change their positions (Fig. 9(f)). It means C–F on the surface of Fe-THC/MXene provided the binding sites for lead sorption. From the above discussion, we can conclude that the OH and F are the main groups of Fe-THC/MXene that provide the sites for the attachment of lead and play an essential role in the adsorption of lead, as shown in Fig. S3.†

3.2.7. Comparative analysis. A comparative analysis was conducted to investigate the potential utilization of Fe-THC/MXene in the rapid, efficient, and selective elimination of lead ions from wastewater. A summary table was established to explain the advantages of the Fe-THC/MXene composite on the rapid, efficient, and selective elimination of lead over other adsorbents based on previous literature. It was concluded that the composite displayed higher adsorption capacity than those previously reported (Table S6†).

4. Conclusion

In this work, we synthesized a novel Fe-THC/MXene for rapid, efficient, and selective removal of lead from wastewater. SEM, TEM, EDS, XRD, FTIR, XPS, and BET were utilized to characterize Fe-THC/MXene. The experiments were performed at distinct pH[1–7] and temperature (305–315 K). At pH 4.5 and 305 K, the adsorption attained sorption equilibrium for 12 min, and the maximum sorption capability was 674 mg g^{-1}. The sorption of Pb^{2+} on Fe-THC/MXene fits the Langmuir isotherm and pseudo-first-order models, which indicates that chemisorption is the rate control step, and the adsorption of Pb^{2+} by Fe-THC/MXene is a single layer on a homogenous surface. From thermodynamic analysis, it can be observed that the sorption phenomena are exothermic, and the sorption is unfavorable as temperature increases. Fe-THC/MXene has a greater affinity for Pb^{2+} ions and can selectively adsorb lead from wastewater. Fe-THC/MXene composite still exhibited a greater elimination rate after five cycles, suggesting that Fe-THC/MXene composite has excellent reusability. Lead mainly interacts with –O and –F ions on the Fe-THC/MXene surface, leading to adsorption.

Author statement

Irfan Ijaz: conceptualization and supervision, writing original draft, reviewing, and editing. Aysha Bukhari: conceptualization, methodology. Ezaz Gilani: resource. Ammara nazir: data curation and investigation. Hina Zain: data curation and investigation.

Conflicts of interest

The authors declare that they have no known competing financial interests or personal relationships that could have appeared to influence the work reported in this paper.

Acknowledgements

All authors acknowledge the School of Chemistry, Minhaj University, Lahore, for providing a platform for this work.

References

1 M. Al-Naimi and M. A. Al-Ghouti, Effects of soaking, acidity and temperature on cadmium and lead removal from rice, *Food Chem.*, 2020, **310**, 125591.

Open Access Article. Published on 15 February 2023. Downloaded on 2/4/2026 7:15:08 PM. This article is licensed under a Creative Commons Attribution-NonCommercial 3.0 Unported Licence.

2 H. A. Naseem, T. Aziz, K. Ahmad, S. Parveen and M. Ashfaq, Rational synthesis and characterization of medicinal phenyl diazenyl-3-hydroxy-1h-inden-1-one azo derivatives and their metal complexes, *J. Mol. Struct.*, 2021, **1227**, 129574.

3 T. Tamiji and A. Nezamzadeh-Ejhieh, Electrocatalytic determination of Hg (II) by the modified carbon paste electrode with Sn (IV)-clinoptilolite nanoparticles, *Electrocatalysis*, 2019, **10**, 466–476.

4 M. Xia, Z. Chen, Y. Li, C. Li, N. Ahmad, W. Cheema, *et al.*, Removal of Hg (II) in aqueous solutions through physical and chemical adsorption principles, *RSC Adv.*, 2019, **9**, 20941–20953.

5 J. Liu, X.-H. Zhang, H. Tran, D.-Q. Wang and Y.-N. Zhu, Heavy metal contamination and risk assessment in water, paddy soil, and rice around an electroplating plant, *Environ. Sci. Pollut. Res.*, 2011, **18**, 1623–1632.

6 P. Szefer, G. Glasby, D. Stüben, A. Kusak, J. Geldon, Z. Berner, *et al.*, Distribution of selected heavy metals and rare earth elements in surficial sediments from the Polish sector of the Vistula Lagoon, *Chemosphere*, 1999, **39**(15), 2785–2798.

7 B. Wu, G. Wang, J. Wu, Q. Fu and C. Liu, Sources of heavy metals in surface sediments and an ecological risk assessment from two adjacent plateau reservoirs, *PLoS One*, 2014, **9**(7), e102101.

8 G. Wang, A. Yinglan, H. Jiang, Q. Fu and B. Zheng, Modeling the source contribution of heavy metals in surficial sediment and analysis of their historical changes in the vertical sediments of a drinking water reservoir, *J. Hydrol.*, 2015, **520**, 37–51.

9 D. Bulgariu and L. Bulgariu, Sorption of Pb (II) onto a mixture of algae waste biomass and anion exchanger resin in a packed-bed column, *Bioresour. Technol.*, 2013, **129**, 374–380.

10 M. Nosuhi and A. Nezamzadeh-Ejhieh, High catalytic activity of Fe (II)-clinoptilolite nanoparticles for indirect voltammetric determination of dichromate: Experimental design by response surface methodology (RSM), *Electrochim. Acta*, 2017, **223**, 47–62.

11 J. Goel, K. Kadirvelu, C. Rajagopal and V. K. Garg, Removal of lead (II) by adsorption using treated granular activated carbon: batch and column studies, *J. Hazard. Mater.*, 2005, **125**(1–3), 211–220.

12 R. G. Pearson, Absolute electronegativity and hardness: application to inorganic chemistry, *Inorg. Chem.*, 1988, **27**(4), 734–740.

13 F. Xiao, L. Fang, W. Li and D. Wang, One-step synthesis of aluminum magnesium oxide nanocomposites for simultaneous removal of arsenic and lead ions in water, *RSC Adv.*, 2015, **5**(11), 8190–8193.

14 S. Mohan, V. Kumar, D. K. Singh and S. H. Hasan, Effective removal of lead ions using graphene oxide-MgO nanohybrid from aqueous solution: isotherm, kinetic and thermodynamic modeling of adsorption, *J. Environ. Chem. Eng.*, 2017, **5**(3), 2259–2273.

15 C. F. Carolin, P. S. Kumar, A. Saravanan, G. J. Joshiba and M. Naushad, Efficient techniques for the removal of toxic heavy metals from aquatic environment: A review, *J. Environ. Chem. Eng.*, 2017, **5**(3), 2782–2799.

16 J.-H. Kwak, M. S. Islam, S. Wang, S. A. Messele, M. A. Naeth, M. G. El-Din, *et al.*, Biochar properties and lead (II) adsorption capacity depend on feedstock type, pyrolysis temperature, and steam activation, *Chemosphere*, 2019, **231**, 393–404.

17 F. Ahmadijokani, S. Tajahmadi, M. Rezakazemi, A. A. Sehat, H. Molavi, T. M. Aminabhavi, *et al.*, Aluminum-based metal-organic frameworks for adsorptive removal of anti-cancer (methotrexate) drug from aqueous solutions, *J. Environ. Manage.*, 2021, **277**, 111448.

18 Green synthesis of iron oxide nanoparticles for lead removal from aqueous solutions, in *Key Engineering Materials*, ed. L. P. Lingamdinne, J. R. Koduru and R. Rao Karri, Trans Tech Publ, 2019.

19 F. Ahmadijokani, H. Molavi, A. Peyghambari, A. Shojaei, M. Rezakazemi, T. M. Aminabhavi, *et al.*, Efficient removal of heavy metal ions from aqueous media by unmodified and modified nanodiamonds, *J. Environ. Manage.*, 2022, **316**, 115214.

20 R. Sinha, R. Kumar, P. Sharma, N. Kant, J. Shang and T. M. Aminabhavi, Removal of hexavalent chromium via biochar-based adsorbents: State-of-the-art, challenges, and future perspectives, *J. Environ. Manage.*, 2022, **317**, 115356.

21 F. Ahmadijokani, S. Tajahmadi, A. Bahi, H. Molavi, M. Rezakazemi, F. Ko, *et al.*, Ethylenediamine-functionalized Zr-based MOF for efficient removal of heavy metal ions from water, *Chemosphere*, 2021, **264**, 128466.

22 G. Lee, C. Chen, S.-T. Yang and W.-S. Ahn, Enhanced adsorptive removal of fluoride using mesoporous alumina, *Microporous Mesoporous Mater.*, 2010, **127**(1–2), 152–156.

23 S. González-Poggini, A. Rosenkranz and M. Colet-Lagrille, Two-dimensional nanomaterials for the removal of pharmaceuticals from wastewater: a critical review, *Processes*, 2021, **9**(12), 2160.

24 X. Zhan, C. Si, J. Zhou and Z. Sun, MXene and MXene-based composites: synthesis, properties and environment-related applications, *Nanoscale Horiz.*, 2020, **5**(2), 235–258.

25 Z. Guo, J. Zhou, L. Zhu and Z. Sun, MXene: a promising photocatalyst for water splitting, *J. Mater. Chem. A*, 2016, **4**(29), 11446–11452.

26 S. K. Nemani, B. Zhang, B. C. Wyatt, Z. D. Hood, S. Manna, R. Khaledialidusti, *et al.*, High-entropy 2D carbide MXenes: TiVNbMoC3 and TiVCrMoC3, *ACS Nano*, 2021, **15**(8), 12815–12825.

27 M. Rosales, A. Garcia, V. M. Fuenzalida, R. Espinoza-González, G. Song, B. Wang, *et al.*, Unprecedented arsenic photo-oxidation behavior of few-and multi-layer Ti3C2Tx nano-sheets, *Appl. Mater. Today*, 2020, **20**, 100769.

28 Y. Wu, H. Chen, J. Xiao, D. Liu, Z. Liu, Y. Qian, *et al.*, Adsorptive Separation of Methanol–Acetone on Isostructural Series of Metal–Organic Frameworks M-BTC (M= Ti, Fe, Cu, Co, Ru, Mo): A Computational Study of Adsorption Mechanisms and Metal-Substitution Impacts, *ACS Appl. Mater. Interfaces*, 2015, **7**(48), 26930–26940.

© 2023 The Author(s). Published by the Royal Society of Chemistry

Open Access Article. Published on 15 February 2023. Downloaded on 2/4/2026 7:15:08 PM. This article is licensed under a Creative Commons Attribution-NonCommercial 3.0 Unported Licence.

29 Y. Dong, D. Sang, C. He, X. Sheng and L. Lei, MXene/alginate composites for lead and copper ion removal from aqueous solutions, *RSC Adv.*, 2019, **9**(50), 29015–29022.
30 P. Zhang, M. Xiang, H. Liu, C. Yang and S. Deng, Novel two-dimensional magnetic titanium carbide for methylene blue removal over a wide pH range: insight into removal performance and mechanism, *ACS Appl. Mater. Interfaces*, 2019, **11**(27), 24027–24036.
31 L. Wang, H. Xu, J. Gao, J. Yao and Q. Zhang, Recent progress in metal-organic frameworks-based hydrogels and aerogels and their applications, *Coord. Chem. Rev.*, 2019, **398**, 213016.
32 C. Wang, X. Liu, N. K. Demir, J. P. Chen and K. Li, Applications of water stable metal–organic frameworks, *Chem. Soc. Rev.*, 2016, **45**(18), 5107–5134.
33 P. A. Kobielska, A. J. Howarth, O. K. Farha and S. Nayak, Metal–organic frameworks for heavy metal removal from water, *Coord. Chem. Rev.*, 2018, **358**, 92–107.
34 F. Ahmadijokani, R. Mohammadkhani, S. Ahmadipouya, A. Shokrgozar, M. Rezakazemi, H. Molavi, *et al.*, Superior chemical stability of UiO-66 metal-organic frameworks (MOFs) for selective dye adsorption, *Chem. Eng. J.*, 2020, **399**, 125346.
35 F. Kong, X. He, Q. Liu, X. Qi, D. Sun, Y. Zheng and *et al.*, Further surface modification by carbon coating for in-situ growth of Fe3O4 nanoparticles on MXene Ti3C2 multilayers for advanced Li-ion storage, *Electrochim. Acta*, 2018, **289**, 228–237.
36 A. Y. Li, H. Deng, Y. H. Jiang, C. H. Ye, B. G. Yu, X. L. Zhou, *et al.*, Superefficient Removal of Heavy Metals from Wastewater by Mg-Loaded Biochars: Adsorption Characteristics and Removal Mechanisms, *Langmuir*, 2020, **36**(31), 9160–9174.
37 W. Plazinski and W. Rudzinski, A Novel Two-Resistance Model for Description of the Adsorption Kinetics onto Porous Particles, *Langmuir*, 2010, **26**(2), 802–808.
38 A. E. Regazzoni, Adsorption kinetics at solid/aqueous solution interfaces: On the boundaries of the pseudo-second order rate equation, *Colloids Surf., A*, 2020, **585**, 124093.
39 I. Langmuir, THE ADSORPTION OF GASES ON PLANE SURFACES OF GLASS, MICA AND PLATINUM, *J. Am. Chem. Soc.*, 1918, **40**(9), 1361–1403.
40 H. Freundlich, Über die Adsorption in Lösungen, *Z. Phys. Chem.*, 1907, **57U**(1), 385–470.
41 M. I. Temkin, Kinetics of ammonia synthesis on promoted iron catalysts, *Acta Physicochim. URSS*, 1940, **12**, 327–356.
42 L. Sun, Q. Fu and C. Pan, Hierarchical porous "skin/skeleton"-like MXene/biomass derived carbon fibers heterostructure for self-supporting, flexible all solid-state supercapacitors, *J. Hazard. Mater.*, 2021, **410**, 124565.
43 A. S. Levitt, M. Alhabeb, C. B. Hatter, A. Sarycheva, G. Dion and Y. Gogotsi, Electrospun MXene/carbon nanofibers as supercapacitor electrodes, *J. Mater. Chem. A*, 2019, **7**(1), 269–277.
44 Y. Zheng, D. Huang and A. Wang, Chitosan-g-poly(acrylic acid) hydrogel with crosslinked polymeric networks for Ni2+ recovery, *Anal. Chim. Acta*, 2011, **687**(2), 193–200.
45 J. Fang, Y. Zhang, S. Yan, Z. Liu, S. He, L. Cui, *et al.*, Poly (L-glutamic acid)/chitosan polyelectrolyte complex porous microspheres as cell microcarriers for cartilage regeneration, *Acta Biomater.*, 2014, **10**(1), 276–288.
46 M. Sivakami, T. Gomathi, J. Venkatesan, H.-S. Jeong, S.-K. Kim and P. Sudha, Preparation and characterization of nano chitosan for treatment wastewaters, *Int. J. Biol. Macromol.*, 2013, **57**, 204–212.
47 K. Wang, N. Wang, J. He, Z. Yang, X. Shen and C. Huang, Graphdiyne nanowalls as anode for lithium—ion batteries and capacitors exhibit superior cyclic stability, *Electrochim. Acta*, 2017, **253**, 506–516.
48 J. Chen, X. Yuan, F. Lyu, Q. Zhong, H. Hu, Q. Pan, *et al.*, Integrating MXene nanosheets with cobalt-tipped carbon nanotubes for an efficient oxygen reduction reaction, *J. Mater. Chem. A*, 2019, **7**(3), 1281–1286.
49 J. Yao, Y. Chen, H. Yu, T. Liu, L. Yan, B. Du, *et al.*, Efficient and fast removal of Pb (II) by facile prepared magnetic vermiculite from aqueous solution, *RSC Adv.*, 2016, **6**(103), 101353–101360.
50 M. Fayazi, Facile hydrothermal synthesis of magnetic sepiolite clay for removal of Pb (II) from aqueous solutions, *Anal. Bioanal. Chem. Res.*, 2019, **6**(1), 125–136.
51 Q. Lian, Z. U. Ahmad, D. D. Gang, M. E. Zappi, D. L. B. Fortela and R. Hernandez, The effects of carbon disulfide driven functionalization on graphene oxide for enhanced Pb (II) adsorption: Investigation of adsorption mechanism, *Chemosphere*, 2020, **248**, 126078.
52 F. K. Mahar, L. He, K. Wei, M. Mehdi, M. Zhu, J. Gu, *et al.*, Rapid adsorption of lead ions using porous carbon nanofibers, *Chemosphere*, 2019, **225**, 360–367.
53 Y. Li, J. Shao, X. Wang, H. Yang, Y. Chen, Y. Deng, *et al.*, Upgrading of bio-oil: removal of the fermentation inhibitor (furfural) from the model compounds of bio-oil using pyrolytic char, *Energy Fuels*, 2013, **27**(10), 5975–5981.
54 X. Min, X. Wu, P. Shao, Z. Ren, L. Ding and X. Luo, Ultra-high capacity of lanthanum-doped UiO-66 for phosphate capture: unusual doping of lanthanum by the reduction of coordination number, *Chem. Eng. J.*, 2019, **358**, 321–330.
55 T. Wu, X. Liu, Y. Liu, M. Cheng, Z. Liu, G. Zeng, *et al.*, Application of QD-MOF composites for photocatalysis: Energy production and environmental remediation, *Coord. Chem. Rev.*, 2020, **403**, 213097.
56 P. Wang, M. Du, H. Zhu, S. Bao, T. Yang and M. Zou, Structure regulation of silica nanotubes and their adsorption behaviors for heavy metal ions: pH effect, kinetics, isotherms and mechanism, *J. Hazard. Mater.*, 2015, **286**, 533–544.
57 M. L. Sall, A. K. D. Diaw, D. Gningue-Sall, A. Chevillot-Biraud, N. Oturan, M. A. Oturan, *et al.*, Removal of lead and cadmium from aqueous solutions by using 4-amino-3-hydroxynaphthalene sulfonic acid-doped polypyrrole films, *Environ. Sci. Pollut. Res.*, 2018, **25**, 8581–8591.

© 2023 The Author(s). Published by the Royal Society of Chemistry